Research Square

Preprints are preliminary reports that have not undergone peer review.
They should not be considered conclusive, used to inform clinical practice,
or referenced by the media as validated information.

Population genetics reveals adaptive signatures of Exidia glandulosa across diverse climates from China

Shubin Liu
Heng Zhao
Wanying Li
Tohtirjap Ablat
Fang Wu
fangwubjfu2014@bjfu.edu.cn

Research Article

Keywords: Climate adaptation, Exidia glandulosa, population genetics, selection signal

Posted Date: November 5th, 2026

DOI: https://doi.org/10.21203/rs.3.rs-11134472/v1

License: This work is licensed under a Creative Commons Attribution 4.0 International License.
Read Full License

Additional Declarations: No competing interests reported.

Abstract

Background

Wood-decaying fungus *Exidia glandulosa*, as the type species of the genus *Exidia*, is widely distributed in China. However, the scarcity of genomic limits the development of subsequent resources mining and utilization.

Results

Here, we firstly assembled the high-quality reference genome of *E. glandulosa* using third-generation and next-generation sequencing technologies, systematically analyzed the population structure and adaptive evolution characteristics of *E. glandulosa* across diverse climatic regions in China based on 78 samples. This assembled genome revealed an abnormally high level of genome heterozygosity, suggesting elevated ancestral genetic diversity or historical inter-lineage hybridization events. Population genetic analyses indicated that genetic differentiation among *E. glandulosa* populations, likely driven by regional climatic variations. Selection signal analysis suggested that temperate populations mainly responded to climate variations through enhancing signal transduction and stress responses, subtropical populations focused on energy metabolism, and plateau populations through multidirectional regulation of pathways including energy sensing, autophagy regulation, and DNA damage repair.

Conclusions

This study elucidates the significant roles of climatic and geographic factors in driving population differentiation and local adaptation in *E. glandulosa*. The rich genetic diversity and flexible molecular regulation mechanisms identified here underpin its wide ecological distribution. Additionally, this work provides a valuable genomic resource for future *Exidia*-related omics research and contributes to birding the gap in studies on climate adaptability of wood-decaying fungi within the framework population genetics.

Introduction

Fungi constitute a vital component of the global biosphere, and among them, wood-decaying fungi act as the primary decomposers of woody substrates in forest ecosystems, exhibiting remarkable species diversity and playing crucial roles in nutrient cycling and ecosystem stability [1, 2, 3, 4, 5, 6]. The intraspecific genetic variation and population structure of wood-decaying fungi are highly responsive to environmental variation, such as climatic conditions, resource quality, and habitat naturalness [7, 8, 9, 10]. Across different climatic zones, precipitation and mean annual temperature are recognized as major factors driving species genetic differentiation [11, 12]. Furthermore, increasing human activities have emerged as one of the primary forces shaping genetic variation in natural populations. Reductions in

host availability and enhanced long-distance spore dispersal driven by human activities may results in population fragmentation, decreased local genetic diversity, and increased population differentiation [13]. Such reductions in genetic diversity may further weaken the potential of species to migrate to new habitats and their ability to adapt to climate change [10].

Fungi rely primarily on spore spread, dispersal, and colonization as fundamental spatial processes underpinning population dynamics [14, 15]. They employ a wide range of dispersal mechanisms, including the transport of both hyphae and spores via air and ocean currents, as well as the use of biological vectors such as plants and animals for short- or long-distance transoceanic dispersal [16]. Dispersal rates largely determine the magnitude and spatial scale of gene flow, thereby shaping population genetic structure and exerting profound influences on interspecific interactions and community assembly [17, 18, 19]. Although adaptive evolution across different habitats is generally shaped by the interplay of gene flow, genetic drift, and natural selection, evidence suggested that natural selection may assume a preeminent role in wood-decaying fungi [10].

Climate is one of the key factors driving the dispersal, diversity, and evolution of forest pathogenic fungi, mycorrhizal fungi, and wood-decaying fungi [20, 21, 22], under whose influence fungi may evolve different evolutionary strategies under varying environmental conditions [23]. In recent years, the use of whole-genome resequencing (WGR) to analyze the adaptive evolution of species to climate change has become an emerging research direction [24]. Related studies have revealed climate-driven selection signatures and local adaptation mechanisms through genome-wide scanning [25, 26]. Currently, fungi population genetics studies mainly focused on the germplasm evaluation and agronomic traits analyses in edible and medicinal species. For example, Cao et al. [27] evaluated the genetic diversity of 18 germplasm resources of *Hymenopellis radicata* (Relhan) R.H. Petersen collected from China. Ling et al. [28] integrated WGR data from 482 wild and commercial strains of *Agaricus bisporus* (J.E. Lange) Imbach worldwide, reconstructing its complex evolutionary and domestication history under historical climatic dynamics, and identifying candidate genes associated with white cap fruiting body traits. However, population genetics and adaptive evolution of wood-decaying fungi across different climatic regions remain notably scarce.

Exidia Fr. is a genus of white-rot fungi belonging to Auriculariaceae, Auriculariales, Agaricomycetes, Basidiomycota. A total of 183 names had been registered for this genus, of which, 96 species are globally recognized, with approximately 10 species reported from China [29, 30, 31, 32]. *E. glandulosa* (Bull.) Fr., the type species of the genus *Exidia*, has been known for more than 200 years (http://www.indexfungorum.org/. Accessed 20 September 2026). To date, research on *E. glandulosa* has largely centered on its industrial applications. For example, Liers et al. [33] investigated dye-decolorizing peroxidase (DyP) EglDyP from *E. glandulosa* and demonstrated that EglDyP could efficiently oxidize non-phenolic aromatic substrates, recalcitrant dyes and the phenolic substrate 2,6-dimethoxyphenol. Sedova et al. [34] and Martínková et al. [35] used the cyanide hydratase (CynH) NitEg, derived from *E. glandulosa* to treat industrial wastewater containing free cyanide (fCN). NitEg is regarded as a promising fCN detoxification biocatalyst due to its ease of preparation, high specific activity, strong stability and long

shelf life. Despite these advances, omics-level studies of *E. glandulosa* remain relatively limited, only a second-generation genome has been reported for this species, which has been used as a reference for comparative analyses of lignocellulose degradation [36, 37] and as an outgroup in phylogenetic analyses of related taxa [38, 39, 40].

Exidia glandulosa is widely distributed in China [29, 41, 42, 43, 44, 45], and represents an ideal model for studying population genetic differentiation and climate-driven adaptive evolution. China exhibits considerable climatic heterogeneity, conventionally demarcated by the Qinling-Huaihe line into a predominantly temperate north and a subtropical south. In addition, Southeast Xizang is characterized by complex and variable climatic conditions, producing diverse forest ecosystems with a forest coverage rate of approximately 46%. As a globally recognized biodiversity hotspot, this area has recently attracted increasing attention in studies of wood-decaying fungi [46, 47].

In this study, we assembled a high-quality genome for *E. glandulosa* and performed WGR of 78 samples to investigate patterns of population differentiation and evolutionary dynamics under contrasting climatic conditions across China. This study not only provides important genomic data for the subsequent multi-omics investigations of *E. glandulosa*-related species, but also fills the gap in the study of climate-driven adaptive evolution in wood-decaying fungi from a population genetics perspective.

Materials and methods

Strain culture and genome sequencing

The *E. glandulosa* strain Dai 21717 used in this study was isolated from basidiomata collected at Saihanba National Forest Park in Weichang Manchu and Mongolian Autonomous County, Chengde City, Hebei Province, China. The specimen was deposited in the herbarium of Beijing Forestry University (BJFC). An axenic single colony was selected, inoculated onto potato dextrose agar (PDA) culture medium plates, and cultured at 25°C in the dark for 1–2 weeks. The genomic DNA from mycelium was extracted using a modified cetyltrimethylammonium bromide (CTAB) method [48]. DNA purity and integrity were assessed by agarose gel electrophoresis. Genome sequencing was performed using the PacBio Sequel II and Illumina NovaSeq PE150 platforms. Library construction and sequencing were performed by Novogene Co., Ltd. (Beijing, China).

A total of 78 basidiomata samples were used for resequencing analysis in this study, of which 72 were collected from 14 provinces or autonomous regions of China, and six were originated from the United States of America (USA) and Europe (Table S1). All specimens are deposited in BJFC. Genomic DNA was extracted using a modified CTAB method [48]. Paired-end sequencing (150 bp) was performed on each sample using the BGI sequencing platform (DNBSEQ-T7) according to the manufacturer's instructions. Library construction and sequencing were performed by Biomarker Co., Ltd. (Beijing, China).

Genome resource quality control and assembly

The raw next-generation sequencing data were evaluated using FastQC v0.12.1 [49] and then filtered by Fastp v0.23.4 [50]. The filtering procedures included removal of adapter sequences, reads with a quality value below 20, reads shorter than 50 bp, and reads containing excessive N bases. *K*-mer analysis was performed on the filtered clean data (k = 17). *K*-mer frequencies were counted using Jellyfish v2.3.0 [51], and genome survey was carried out using GenomeScope v2.0 [52].

Third-generation sequencing data were assembled using Canu v2.2 [53] and SMRT Link v5.0.1 [54]. The genome of *E. glandulosa* (HHB12029) was selected as the reference, with an estimated genome size of 75 Mb. After assembly, contigs were aligned to the third-generation data using minimap2 v2.24-r1122 [55], and redundant sequences were removed using purge_dups v1.2.5 [56]. Multiple rounds of assembly merging were subsequently performed using Quickmerge v0.3 [57, 58]. To improve assembly accuracy, four rounds of polishing and error correction were performed on the Quickmerge v0.3 assembly using NextPolish v1.4 [59] with both third-generation and filtered next-generation reads. Contigs shorter than 300 kb were manually removed using SeqKit v2.2.0 [58, 60] to obtain the final genome. The genome quality and completeness were evaluated using QUAST v5.0.2 [61] and BUSCO v5.2.0 [62] with the fungi_odb10 database.

Genome prediction and annotation

Genome repeat sequences were identified using both homology-based and *de novo* approaches. For homology-based detection, RepeatMasker v4.1.4 and RepeatProteinMask v4.1.4 [63] were employed against the RepBase (https://www.girinst.org/repbase/) and Dfam (https://www.dfam.org/home/) databases. Long terminal repeats (LTRs) were detected using LTRharvest (http://genometools.org/), LTR_FINDER v1.0.7 [64], and LTR_retriever v2.9.0 [65], masked during homology-based annotation. For *de novo* prediction, RepeatModeler v2.0.3 [66] was used, followed by tandem repeat prediction with TRF v4.0.9 [67]. All annotation outputs were merged into the final repeat annotation set.

Non-coding RNA (ncRNA) annotation was performed with Infernal v1.1.4 [68] based on the Rfam database (https://rfam.org/). rRNA and tRNA were predicted using RNAmmer v1.2 [69] and tRNAscan-SE v2.0.9 [70], respectively. The rRNA and tRNA sequences identified by Infernal were then screened and combined with the RNAmmer v1.2 and tRNAscan-SE v2.0.9 outputs to produce the final ncRNA annotation results.

To reduce the impact of repetitive elements on gene structure annotation, repetitive sequences in the genome were masked using bedtools v2.30.0 [71]. Gene prediction integrated *ab initio* prediction with Augustus v3.3.3 [72] and homology-based annotation with GeMoMa v1.9 [73]. The prediction results were integrated using EVM v1.1.1 [74]. Completeness of the final gene was assessed using BUSCO v5.2.0 [62] with the fungi_odb10 database.

Variation detection and annotation

The genome of *E. glandulosa* (Dai 21717) was used as the reference genome. Filtered reads were aligned to the reference genome using BWA v0.7.17-r1188 [75], and the resulting alignments were converted into BAM files. Picard v3.0.0 (http://broadinstitute.github.io/picard/) was then employed to sort BAM files and remove PCR duplicates. BAM files indexing was performed with Samtools v1.18 [76]. Alignment statistical was generated using QualiMap v2.3 [77], including total reads, mapping rate, coverage rate, duplication rate, and insert size.

Variant calling for single nucleotide polymorphisms (SNPs) and insertion-deletion polymorphisms (indels) was performed using HaplotypeCaller module in GATK v4.4.0 [78]. The low-quality SNPs and indels were filtered using VariantFiltration module [28]. Indels located around SNPs were further filtered using the script tool vcfutils.pl (https://github.com/lh3/samtools/blob/master/bcftools/vcfutils.pl). Soft filtering was performed using VCFtools v0.1.16 [28, 79]. The filtered files were then separated with VCFtools v0.1.16 to obtain high-quality SNP and indel datasets. Annotation of SNPs and indels was conducted using ANNOVAR [80] to determine variation types, affected genes, and genomic regions.

Population structure and evolution analysis

The high-quality SNP data in VCF format were converted to Phylip format using the run_pipeline.pl command in TASSEL v5.2.90 [81]. A Maximum Likelihood (ML) phylogenetic tree was construct using RAxML-NG v1.1.0 [82], *Auricularia cornea* Ehrenb. (Dai 24584; SRA accession: SRR38361196) and *A. subglabra* Looney, Birkebak & Matheny (TFB10046; SRA accession: SRR3927431) [83] were used as outgroups, and the bootstrap value was set to 1,000. Finally, the resulting phylogenetic tree was visualized and edited using FigTree v1.4.4 (http://tree.bio.ed.ac.uk/software/figtree) and iTOL (https://itol.embl.de/).

Principal component analysis (PCA) was performed using PLINK v1.90 [84] based on high-quality SNP data. The number of principal components (PC) was set to five and eight according to the population structure. Linkage disequilibrium (LD) pruning was performed in PLINK v1.90 by calculating the squared correlation coefficient (r^2) between SNP pairs within a sliding window of 50 SNPs, with a step size of 10 SNPs; SNPs with $r^2 > 0.2$ were removed. Population structure of the filtered SNPs was inferred using ADMIXTURE v1.3.0 [85], with the number of clusters (K) tested up to ten. The optimal K value was determined by minimizing the cross-validation (CV) error. LD decay was analyzed using PopLDdecay v3.40 [86], and gene flow among populations was inferred with TreeMix v1.13 [87]. Visualization of the above results was carried out using R packages.

Selective sweep analysis

VCFtools v0.1.16 was used to calculate the genetic diversity (Pi), the Tajima's D value, and the fixation index (Fst) of each population with a 20 kb window size and a 5 kb step size. The Fst and Pi values were combined to screen the selected regions, and the first 5% of the results were selected as the selected regions [88]. For the Tajima's D value, regions showing significant deviation from zero were emphasized:

significantly positive values may indicate bottlenecks or balancing selection, whereas significantly negative values may reflect population expansion or directional selection [89].

The Python version of XP-CLR (https://github.com/hardingnj/xpclr) was used to calculate the frequency difference of multiple sites, and the first 1% region was selected as the selected region of the genome [90]. Protein-coding genes (PCGs) residing within these selected regions were extracted using bcftools v1.18 [91] and subsequently subjected to functional annotation using the eggNOG database [92]. The above analysis results were visualized using R packages.

Results

Genome survey and components of Exidia glandulosa

The *E. glandulosa* Dai 21717 was sequenced using the PacBio and Illumina platforms, generating a total of 5.8 Gb of raw data. The mean quality value of each base position in the reads of *E. glandulosa* ranged from 35.03 to 36.31, the GC content was 57%, and the proportion of repeat sequences in forward and reverse reads was 16.6% and 16.1%, respectively, according to the FastQC v0.12.1. *K*-mer analysis revealed that the maximum coverage depth of *E. glandulosa* was 25.5×, the estimated genome total length was 71.56 Mb, and the heterozygosity rate was 5.48% (Fig. S1). The assembly results from different software were compared, and the best assemblies were selected for merging to obtain the final assembly. The final assembly had a total length of 71.63 Mb, with a GC content of 56.58%, which was close to the genome survey estimate (Fig. 1). Compared with the previously published *E. glandulosa* (HHB12029) assembly, the number of contigs in the present assembly decreased from 1,727 to 75, N50 increased from 0.12 kb to 1.31 Mb, and L50 declined from 181 to 17. BUSCO evaluation gave a genome completeness score of 91.0% (Table 1).

Gene annotation was performed by combining homology-based annotation and *ab initio* prediction. The total length of repetitive sequences in the *E. glandulosa* genome was 14.97 Mb, accounting for 20.9% of the genome size. Among these, LTRs constituted the highest proportion, at 10.87%. A total of 261 ncRNAs was annotated, including 27 snRNAs, 26 rRNAs, and 208 tRNAs. 19,142 PCGs were predicted based on *ab initio* and homology-based methods. BUSCO evaluation gave a genome annotation completeness score of 94.20% (Table 1).

Table 1
Statistics of the genome assembly and component of *Exidia glandulosa*.

Species	***Exidia glandulosa***	
Sample no.	Dai 21717	HHB12029
Genome size (Mb)	69.46	75.64
Contigs	72	1,727
N50 (Kb)	1,312,362	117,273
L50	17	181
Repeat Stats (%)	20.90%	10.00%
ncRNA	261	300
BUSCOs in assembly (%)	91.00%	92.10%
GC (%)	56.58	56.66
BUSCOs in annotation (%)	94.20%	92.40%
Protein-coding genes	19,142	22,243

Resequencing analyses and detection of variant sites

The morphology of *E. glandulosa* basidiomata is variable, exhibiting different forms even under the same climatic conditions (Fig. 2). To explore the adaptive evolutionary strategies of *E. glandulosa* across diverse habitats, 78 samples collected from different climatic regions were sequenced on the BGI sequencing platform, generating more than 2 Gb of data per sample. The quality control report showed that Q20 ranged 95.47% from 98.64%, Q30 from 92.97% to 97.63%, and the GC content from 55.04% to 59.09% (Table S1). Genomic survey analysis based on resequencing data revealed that the heterozygosity level ranged from 2.30% to 6.57% (Table S1), indicating that a high degree of genomic complexity in this species.

In this study, the genome of *E. glandulosa* Dai 21717 assembled was used as the reference genome for read alignment. The resequencing data were mapped to the reference genome, and alignment statistics generated by QualiMap v2.3 showed that mapping rates ranged from 38.94% to 78.54%, average sequencing depth from 20.16× to 54.51×, and the average genome coverage ranged from 70.46% to 88.26% (Table S1). These results suggest a considerable divergence between the sampled individuals and the reference genome.

A total of 31,675,338 variant sites were detected from 78 samples using GATK v4.4.0. After stringent filtering, 36,661 high-quality variant sites were retained, including 21,051 high-quality SNPs and 15,610 high-quality indels, which were extracted by VCFtools v0.1.16. These variants were annotated using

ANNOVAR. The results indicated that both SNPs and indels were most densely distributed on Contig 14. SNPs were predominantly located in exonic regions, with the majority representing synonymous mutations (Fig. S2A). Among these sample, Wu 263 exhibited the fewest number SNPs (4,907), whereas Dai 23207 had the most number SNPs (10,227). The predominant mutation types were C:G > T:A and T:A > C:G transitions (Fig. S2B), with transition counts ranged from 3,901 to 7,974, and transversions ranged from 1,006 to 2,253. Indels were primarily distributed in upstream and intronic regions (Fig. S3). The number of indels ranged from 3,615 (sample Dai 23671) to 7,364 (sample Dai 23207). In both exonic regions and the whole genome, insertion and deletion lengths were predominantly 1–3 bp. Notably, 3 bp indels were the most frequent in exonic regions, whereas 1 bp indels were the most common genome-wide (Fig. S4).

Population structure and phylogeny of Exidia glandulosa

Auricularia cornea Dai 24584 and *A. subglabra* TFB 10046 were selected as outgroups, and a total of 25,556 high-quality SNPs were obtained for phylogenetic analysis. A ML tree was constructed using RAxML-NG v1.1.0 (Fig. 3). Integrating phylogenetic results with habitat information, the 78 samples were divided into five populations: (1) Temperate I: consisting of eight samples from Xinjiang, Europe, and USA, which formed an independent clade. (2) Temperate II: located at the base of the phylogenetic tree, comprising 30 samples from the northern and northeastern temperate regions China. (3) Transitional: composed of 11 samples from the temperate–subtropical transition zones, which formed a partially distinct clade while some samples were interspersed among other groups. (4) Subtropical: comprising 15 samples from subtropical region of southern China, which clustered into two phylogenetic clades. (5) Plateau: consisting of 14 samples from the southwestern plateau region of China (Xizang and Yunnan plateau), which formed a separate clade in the phylogenetic tree.

PCA was performed based on 21,051 high-quality SNPs after filtering (Fig. 4A). The first two principal components explained 37.65% and 13.21% of the total genetic variation, respectively. When interpreted in conjunction with the population structure inferred from phylogenetic analysis, the positions of individual samples in the PCA plot were clearly resolved. PC2 distinguished the Temperate I population from the other three populations (Temperate II, Transitional, and Subtropical), which clustered more closely and exhibited a linear distribution pattern. In addition, when integrated with the regional distribution data, the 78 samples subdivided into eight finer-scale subpopulations (Fig. 4B): the Temperate I population was divided into Eurasian and USA subpopulations; the Subtropical population was split into South China and South Yunnan subpopulations; and the Plateau population was divided into Xizang and Yunnan Plateau subpopulations.

Population structure was inferred using ADMIXTURE v1.3.0, with population assignment interpreted in conjunction with the phylogenetic topology and PCA results (Fig. 4C). At K = 2, the Plateau group was clearly separated from the other populations. At K = 3, the Temperate I population began to diverge. At K = 4, distinct genetic components of the Subtropical population appeared, and the Transitional population displayed intermediate characteristics between temperate and subtropical; at this K value, the population

partitioning was consistent with the five major groups identified by phylogenetic analysis. At K = 5, the USA subpopulation began to diverge. For K = 6–8, increasing K value revealed progressively greater admixture among populations; however, the genetic compositions of Eurasian and Xizang subpopulations remained relatively stable, suggesting that these populations have undergone independent differentiation within their respective habitats.

Patterns of population differentiation in Exidia glandulosa

LD analysis showed significant differences in LD decay rates among populations (Fig. 5A). The Temperate I and Plateau populations exhibited the slowest LD decay, suggesting that these populations may have experienced recent bottleneck effects or strong genetic drift. This pattern is consistent with the admixture results that their genetic components remained stable at K = 6–8. In contrast, the Temperate II population show the fastest LD decay, followed by the Subtropical population, indicating larger effective population sizes or higher recombination rates in these groups. It is worth noting that the Transitional population shows relatively slow decay rate, which may be reflect its mixed internal components of the Transitional population, as some individuals are genetically closer to temperate populations, whereas others are more similar to subtropical populations, resulting in a lower average LD decay rate.

The Fst and Pi values among populations of *E. glandulosa* were calculated (Fig. 5B). The Plateau population harbored a relatively high level of genetic diversity (Pi: 8.90×10^{-5}), significantly exceeding that of other populations, and possessed more abundant SNPs than other populations, indicating substantial genetic divergence among *E. glandulosa* individuals under long-term selection pressure in the plateau environment. In addition, the Plateau and Temperate I populations showed higher Fst values than other populations, suggesting pronounced genetic differentiation. This pattern likely reflects their relatively independent evolutionary histories and prolonged limitation of gene flow with other populations.

TreeMix analysis revealed three gene flow events among all populations of *E. glandulosa* (Fig. 5C). The Transitional population contributed gene flow to both the Temperate II and Plateau populations, with a higher migration signal associated with the latter. Additionally, a substantial gene flow was detected from the Plateau population to the Subtropical population. However, population structure analysis show that the Xizang subpopulation within the Plateau population consistently maintained an independent genetic component, with no evidence of admixture with other populations.

To further investigate the internal heterogeneity within the Plateau population, the Temperate I and Temperate II populations were excluded, and the TreeMix analysis was repeated based on the five subpopulations identified from the structure analysis (Fig. 5D). The results showed that the gene flow between the Yunnan Plateau subpopulation and both the South Yunnan and Transitional subpopulations, as well as between the Transitional and South China subpopulations. These findings suggest that the previously inferred gene flow from the Transitional to the Plateau population predominantly occurred between the Transitional and Yunnan Plateau subpopulations, whereas the Xizang subpopulation, similar

to the Temperate I population, maintained an independent evolutionary trend with little or no gene exchange. This interpretation is highly consistent with the phylogenetic tree, in which Xizang and Temperate I form distinct clades, and with the PCA results, where both populations are clearly separated from the remaining populations.

Functional differentiation and dynamic patterns of selection signals in the temperate and subtropical populations of Exidia glandulosa

To explore differences in adaptive evolution of *E. glandulosa* between temperate and subtropical habitats, joint Fst and Pi screening was performed, and 33 and 43 candidate regions were detected in the Temperate II and Subtropical populations, respectively (Fig. 6A). In the Temperate II population, these regions were more dispersed across the genome, whereas in the Subtropical population, 30 regions were enriched on Contig 2 and Contig 16. From these regions, 82 and 215 PCGs were extracted from the Temperate II and Subtropical populations, respectively. As a complementary approach to capture recent or ongoing selection signals. XP-CLR analysis, using the Transitional population as a reference, detected 25 selected regions in both Temperate II and Subtropical populations (Fig. 6B and 6C), and extracted 158 and 137 PCGs from them, respectively. The Kyoto Encyclopedia of Genes and Genomes (KEGG) and Gene Ontology (GO) databases were subsequently used to annotate the functions of the extracted PCGs.

KEGG annotation from the joint Fst and Pi screening showed clear ecotype-specific differentiation in selective targets at the molecular pathway level between the two populations (Fig. 7A and 7C). At the level of signal transduction, the two populations are concentrated in the mitogen-activated protein kinase (MAPK) and other signaling pathways, but the executive genes were different. The Temperate II population was characterized by enrichment of p21-activated kinase 1 (PAK1), whereas the Subtropical population was characterized by Ras-related C3 botulinum toxin substrate 1/Ras-related C3 botulinum toxin substrate 3 (RAC1/RAC3; Table S2 and S4). The two populations exhibited pronounced differences at the core metabolic level. In the Temperate II population, selection signals primarily pointed to endocytosis and its coupling with signal transduction, whereas those in the Subtropical population were more concentrated on thermogenesis and the oxidative phosphorylation pathway of cellular energy metabolism—pathways not detected in the Temperate II population (Table S2 and S4).

The overall trend of KEGG annotation results from the XP-CLR analysis was similar to that observed in the joint Fst and Pi screening, though with certain dynamic shifts (Fig. 7E and 7G). The Temperate II population remained dominated by signal transduction and stress response pathways, but the dominant genes in the MAPK and other signaling pathways changed from PAK1 to RAC1/RAC3. In addition, metabolic pathways such as glycolysis/gluconeogenesis are also implicated. The Subtropical population continued to exhibit a pronounced bias toward energy metabolism and ion transport. Oxidative phosphorylation was the most prominent commonly annotated pathway, linked to the cyclic adenosine monophosphate (cAMP) and Cyclic Guanosine monophosphate-dependent protein kinase G (cGMP-PKG) signaling pathways via sodium/potassium-transporting ATPase subunit alpha (ATP1A). At the metabolic level, starch and sucrose metabolism and terpenoid backbone biosynthesis were highlighted,

and organelle-related pathways such as endocytosis. Notably, although the Temperate II population showed a lack of oxidative phosphorylation in the joint Fst and Pi screening, the XP-CLR analysis detected an oxidative phosphorylation pathway mapped by F-type H^+-transporting ATPase subunit d (ATPeF0D) and V-type H^+-transporting ATPase 21kDa proteolipid subunit (ATPeV0B; Table S6 and S8).

GO annotation from the joint Fst and Pi screening also revealed substantial differences between the Temperate II and Subtropical populations (Fig. 7B and 7D). In the Temperate II population, selection signals were highly enriched in terms related to signal regulation and stress response, such as response to stress, response to chemical, and multiple positive regulation. In contrast, in the Subtropical population, selection signals spanned a broad range of basic metabolic and structural maintenance terms, including intracellular anatomical structure, organelle, and cellular metabolic process (Table S3 and S5). The GO annotation results from the XP-CLR analysis differed from those obtained in the joint Fst and Pi screening (Fig. 7F and 7H): the Temperate II and Subtropical populations displayed high consistency, with both focusing on intracellular anatomical structure, organelle, cytoplasm, and various fundamental metabolic processes (Table S7 and S9).

Adaptive selection characteristics of Exidia glandulosa in plateau habitat

The plateau region represents a unique and extreme habitat, and the *E. glandulosa* populations inhabiting this environment exhibit distinct genetic characteristics. To investigate these patterns, we performed joint Fst and Pi analyses comparing the Plateau population with the Temperate II and Subtropical populations (Fig. 8A and 8B). Three unique candidate selection regions in Plateau population were identified, form which 26 PCGs were extracted. Tajima's D analysis was further conducted to infer recent demographic and selective events within the Plateau population (Fig. 8C). Notably, no significant negative regions were detected in the Plateau population, but 175 regions with significantly positive Tajima's D were identified, yielding 120 PCGs. This pattern suggests that the Plateau population may have experienced recent bottleneck effects or balancing selection events.

Functional annotations of PCGs from both joint Fst, Pi analysis, and the Tajima's D analyses revealed partially overlapping yet distinct patterns (Fig. 8D and 8F). In the KEGG results from the joint Fst and Pi analysis mainly highlighted pathways related to AMP-activated protein kinase (AMPK) signaling pathway and autophagy–yeast. Key genes, such as calcium/calmodulin-dependent protein kinase 2 (CAMKK2)/SNF1-activating kinase 1 (SAK1), function as upstream activator of sucrose non-fermenting 1-related protein kinase 1 (SNF1)/AMPK kinase and were associated with the longevity regulating pathway. Additional annotations, including ABC transporters and ubiquitin-mediated proteolysis, suggested the involvement of transmembrane transport and protein degradation (Table S10).

In contrast, the Tajima's D analysis identified a larger and more functionally diverse gene set, encompassing multiple signaling pathways, such as the MAPK signaling pathway, as well as protein degradation and DNA repair related pathways, such as Ubiquitin mediated proteolysis (Table S12). Overall, the results of the joint Fst and Pi analysis primarily highlighted AMPK/SNF1-mediated energy

sensing and autophagy, whereas the Tajima's D analysis revealed a wider array of functional categories, including signal transduction, DNA damage repair, protein degradation, and cell wall synthesis.

In the GO functional annotation results, partial overlap was observed between the two approaches, although their functional emphases differed (Fig. 8E and 8G). The annotations derived from the joint Fst and Pi analysis primarily encompassed intracellular structures, basal metabolic processes, signal transduction, and cellular responses to stimuli, with membrane-associated terms also represented (Table S11). The Tajima's D analysis yieded a larger number of genes, and in addition to the shared categories, further included items related to cell cycle regulation, stress responses, the inner membrane system, and negative regulation of metabolic and biological processes (Table S13).

Discussion

Exidia glandulosa has a complex genetic background

A high-quality reference genome is an essential prerequisite for population genetic analysis. Since Nagy et al. [36] firstly reported the second-generation genome of *E. glandulosa*, the study of *Exidia* intragenus genomics has almost stagnated. Currently, only the second-generation assembled genome sequence of *E. glandulosa* is available in major public databases (https://www.ncbi.nlm.nih.gov/; https://genome.jgi.doe.gov/portal/), a limitation that greatly hinders the advancement of population genetic research in this genus. The genome of *E. glandulosa* (Dai 21717) obtained in this study has been significantly improved compared with previously published genomes, and this high-quality genome provides an important basis for future research on population genetics and other omics-level studies within the genus *Exidia*.

In the life cycle of Basidiomycota fungi, most species exhibit a dikaryotic stage with clamp connections as the primary vegetative growth stage [93, 94]. The dikaryon represents a typical heterokaryotic form, in which a single mycelial cell contains two compatible haploid nuclei [95]. Owing to this heterokaryotic state, Basidiomycota fungi display complex genetic characteristics during the dikaryon stage. Genome-wide heterozygosity is essentially derived from allelic differences between the two parental haploid nuclei and directly reflects the degree of genetic differentiation between them. In previous studies, *A. bisporus*, *Porodaedalea mongolica* Y.D. Wu & Y. Yuan, and *Daedaleopsis sinensis* (Lloyd) Y.C. Dai generally maintain a low level of genomic heterozygosity at the dikaryotic stage, ranging from 0.5% to 2.5%, which is significantly lower than that of *E. glandulosa* [28, 58, 96]. This exceptionally high heterozygosity indicates substantial genetic divergence between the two parental haploid nuclei of *E. glandulosa*, potentially reflecting elevated ancestral genetic diversity or recent hybridization events among divergent genetic lineages. Moreover, higher heterozygosity may enhance environmental adaptability to *E. glandulosa*, facilitating its broad distribution and survival across diverse habitats [97, 98, 99].

Climate is the main factor affecting the population differentiation of Exidia glandulosa

Phylogenetic analysis plays an important role in ecological and evolutionary biology, which can be used to reveal the key processes, such as lineage origin, diffusion path and ancestral trait differentiation [100]. In this study, the Temperate II population was located at the base of the phylogenetic tree, suggesting that it may represent the earliest lineage to have diverged from the common ancestor. The dry and windy climate characteristic of temperate regions is considered conducive to long-distance spore dispersal [101], which may indirectly accelerate the rate of LD decay in the Temperate II population. In addition, the Temperate II population had similar Pi levels and lower Fst values with the Transitional and Subtropical populations. PCA results further revealed a linear distribution pattern, and clear evidence of gene flow was detected among these populations. Collectively, these findings indicate that the three populations likely belong to the same genetic lineage during evolution, but exhibit divergent evolutionary trajectories shaped by distinct climatic regimes.

Both the Temperate I and Plateau populations had followed relatively independent evolutionary trajectories. The samples from Xinjiang, China, within the Temperate I population did not exhibit the genetic components observed in other Chinese populations and clustered with European samples in the population structure analysis, implying that the ancestors of this population may have originated in Europe.

Southwest China (especially Yunnan Province) has become the region with the most abundant fungal diversity in China due to its complex climatic, geological and geographical background [102, 103]. Correspondingly, the Yunnan Plateau subpopulation (belonging to Plateau population) in northwestern Yunnan and the South Yunnan subpopulation (belonging to Subtropical population) in southern Yunnan showed significant differences in genetic composition. In the phylogenetic tree, the Plateau and Subtropical populations clustered within the same clade, suggesting that the ancestors of the Xizang subpopulation may have originated in subtropical regions and subsequently dispersed to their current distribution range via northwestern Yunnan.

In addition to climatic factors, human activities also act as an important factor of population differentiation. The distribution areas of the Temperate II, Transitional, and Subtropical populations have high population density and frequent anthropogenic activity. As population density and forest utilization intensity increase, the proportion of local old-growth forest declines, which may lead to reduced genetic diversity in these regions [10, 104]. Host factors also constitute a key variable influencing fungal distribution patterns [105]. However, this effect may be more pronounced in host-specific taxa, such as *Sanghuangporus* Sheng H. Wu, L.W. Zhou & Y.C. Dai species [106]. As a widely distributed species, *E. glandulosa* exhibits a wide host range. In this study, host information for the sequenced samples was systematically compiled (Table 2), and no obvious host specificity or significant host-driven genetic differentiation was found in *E. glandulosa*.

Different adaptive evolution trends of Exidia glandulosa in temperate and subtropical climates

Under different climatic conditions, the differentiation of species is driven by natural selection, and the degree of differentiation depends on the intensity and type of selective pressure [24]. In the joint Fst and

Pi selected regions, PAK1 in the Temperate II population is involved in the regulation of the cytoskeleton and mitosis [107, 108, 109, 110], whereas RAC1/RAC3 in the Subtropical population plays an important role in regulating actin cytoskeleton organization and controlling cell polarity across diverse organisms [111, 112, 113]. The MAPK cascade pathway involved in PAK1 and RAC1/RAC3 can mediate the response of cells to external stimuli, thereby regulating the adaptation to various biotic and abiotic stresses encountered in the natural environment [114]. In the GO functional annotation, the Temperate II population was also enriched for multiple stress response and positive regulation terms, whereas the Subtropical population was enriched for more terms related to basal metabolism and cell structure maintenance.

Furthermore, the genes under selection in the Temperate II population were predominantly involved in endocytosis, a process that enables cells to quickly adapt to fluctuating environments by selectively removing plasma membrane transporters [115, 116]. In contrast, oxidative phosphorylation, which was under biased selection in the Subtropical population, is the main energy-producing pathway in eukaryotes [117, 118]. It is worth noting that thermogenesis, as a high-energy-consuming pathway, also exhibited clear selection signals. However, due to the lack of relevant research on thermogenesis in fungi, its specific role remains uncertain, but there are many subordinate pathways related to thermogenesis in the Subtropical population. These characteristics may reflect that *E. glandulosa* has a longer growing season in the subtropical environment, faster growth rate, and requires a greater heat supply.

In the recent selection signals identified by XP-CLR analysis, the dynamic changes were characterized by a shift in dominant genes. The dominant signal transduction gene in the Temperate II population shifted from PAK1 to RAC1/RAC3, and a necessary physical interaction exists between RAC and PAK. PAK can directly bind to phosphoglycerate mutase and inhibit its activity, thereby redirecting RAC from glycolysis toward the pentose phosphate pathway and consequently enhancing cellular antioxidant capacity [119, 120].

Unique selection signatures of Exidia glandulosa in plateau environment

High-altitude environment has the typical characteristics of high ultraviolet radiation intensity, low temperature, and low oxygen content [121, 122]. In order to survive in such a complex environment, plateau species have evolved effective adaptive strategies at the genomic level to cope with various environmental stresses [123]. *E. glandulosa* also exhibited distinctive genetic characteristics in the plateau environment, achieving multi-faceted adaptation to various environmental stresses through balancing selection that maintains genetic polymorphism.

In the *E. glandulosa* Plateau population, SAK1/CAMKK2 is mapped to the longevity regulating pathway as an upstream activator of SNF1/AMPK kinase. Activation of AMPK can stimulate various catabolic processes, including autophagy [124]. SNF1 not only participates in autophagy induction but also affects the lifespan of species [125, 126]. The research on the longevity regulating pathway in Basidiomycota fungi is relatively limited, but it has been confirmed in yeast that this pathway can modulate cellular

lifespan [127]. Under environmental stress in particular, fungus may adopt an S-strategy and achieve the best growth status by reducing mycelial growth rate and enhancing persistence to withstand adverse conditions [128]. Under stressful conditions such as drought, autophagy helps fungal adaptation to extreme environments and maintenance of cellular homeostasis by mediating the degradation and recycling of intracellular waste to generate energy and meet basal metabolic demands [129].

The recent selection signals revealed by Tajima's D analysis covered a broader functional spectrum. Among them, the MAPK cascade pathway is widely recognized as a core pathway through which fungi respond to external stimuli and regulate diverse environmental stress responses. DNA damage repair pathways such as Nucleotide excision repair (NER) and Base excision repair (BER) represent the major molecular mechanisms by which fungi counteract DNA damage induced by ultraviolet radiation and oxidative stress [130]. Furthermore, the annotation of ABC transporters and ubiquitin mediated proteolysis by both analytical approaches suggests that selective protein degradation via the ubiquitin-proteasome system participates in the adaptive evolution of the Plateau population. The pivotal role of the ubiquitin-proteasome system in fungal responses to various stresses has been well established [131].

Conclusions

In this study, a high-quality reference genome of *E. glandulosa* was assembled for the first time, and the population structure and adaptive evolution trends of this species across different climatic regions of China were systematically analyzed based on WGR data. The results showed that *E. glandulosa* exhibited abnormally high genomic heterozygosity, suggesting that its ancestral had rich genetic diversity or historical inter-lineage hybridization events. Population genetic analysis revealed that the Temperate II, Transitional, and Subtropical populations belong to the same genetic lineage but displayed divergent evolutionary trends under different climatic regimes, whereas the Temperate I and Plateau populations maintained relatively independent evolutionary paths.

Selection signal analysis further showed that, in temperate environments, *E. glandulosa* has primarily reinforced signal transduction, endomembrane transport, and stress response functions to cope with climatic variability. In subtropical environments, it emphasizes energy metabolism pathways to maintain high metabolic efficiency. In the Plateau population, long-term selection signals converged on energy sensing and autophagy regulatory pathways, while recent selection extended to DNA damage repair, stress response, and multiple signaling pathways, reflecting the all-round shaping of *E. glandulosa* from basic survival guarantee to diversified regulatory networks in the extreme environment of the plateau.

In summary, population differentiation and local adaptation in *E. glandulosa* are strongly driven by climatic and geographical factors. Its abundant genetic diversity and flexible molecular regulatory strategies provide an important genetic foundation for the broad distribution of this species across heterogeneous habitats.

Declarations

Ethics approval and consent to participate

Not applicable.

Consent for publication

Not applicable.

Data availability

The genome assembly of *E. glandulosa* (Dai 21717) has been deposited in the NCBI database under BioProject accession PRJNA1457268. The WGR data have also been deposited in the NCBI database, with the SRA accession numbers provided in Table S1.

Competing interests

The authors declare no competing interests.

Funding

This study was financed by the National Natural Science Foundation of China (Project Nos. 32570008 & 32270011), and the Fundamental Research Funds for the Central Universities (No. QNTD202509).

Authors' contributions

Shubin Liu: Data curation, Formal analysis, Methodology, Software, Visualisation, Writing-original draft, Writing-review and editing. Heng Zhao: Methodology, Conceptualisation, Writing-review and editing. Wanying Li: Investigation, Data curation. Ablat Tohtirjap: Investigation, Data curation. Fang Wu: Conceptualisation, Funding acquisition, Writing-review and editing.

Authors' information

1 School of Ecology and Nature Conservation, Beijing Forestry University, Beijing 100083, China

2 CAS Key Laboratory of Forest Ecology and Silviculture, Institute of Applied Ecology, Chinese Academy of Sciences, Shenyang 110016, China

3 College of Life Sciences, Shihezi University, Shihezi 832003, China

References

1. Stokland JN, Siitonen J, Jonsson BG. Biodiversity in dead wood. Cambridge: Cambridge University Press; 2012. pp. 1–509.

2. Heilmann-Clausen J, Aude E, Van Dort K, et al. Communities of wood-inhabiting bryophytes and fungi on dead beech logs in Europe-reflecting substrate quality or shaped by climate and forest conditions? J Biogeogr. 2014;41:2269–82. https://doi.org/10.1111/jbi.12388.
3. Kahl T, Arnstadt T, Baber K, et al. Wood decay rates of 13 temperate tree species in relation to wood properties, enzyme activities and organismic diversities. For Ecol Manag. 2017;391:86–95. https://doi.org/10.1016/j.foreco.2017.02.012.
4. Xue JB, Chen LT, Wei YL. Research progress on functional traits of wood-decaying fungi in forest ecosystem. Chin J Ecol. 2024;43(9):2587–95. https://doi.org/10.13292/j.1000-4890.202409.008.
5. Zhao H, Cui YJ, Guan QX, et al. Global species diversity and distribution patterns within the order Hymenochaetales (Agaricomycetes, Basidiomycota). Mycosphere. 2025;16(1):3257–80. https://doi.org/10.5943/mycosphere/16/1/24.
6. Zhao H, Yuan HS, Cui YJ, et al. Global polypore diversity and distribution patterns. Fungal Divers. 2026;136:136002. https://doi.org/10.65390/fdiv.2026.136002.
7. Abrego N, Salcedo I. Research of wood-inhabiting fungal community to fragmentation in a beech forest landscape. Fungal Ecol. 2014;8:18–27. https://doi.org/10.1016/j.funeco.2013.12.007.
8. Juutilainen K, Monkkonen M, Kotiranta H, Halme P. Research use of wood-inhabiting fungi in different boreal forest types. Fungal Ecol. 2017;27:96–106. https://doi.org/10.1016/j.funeco.2017.03.003.
9. Pouska V, Macek P, Zibarova L, Ostrow H. How does the richness of wood-decaying fungi relate to wood microclimate? Fungal Ecol. 2017;27:178–81. https://doi.org/10.1016/j.funeco.2016.06.006.
10. Sønstebø JH, Trucchi E, Nordén J, et al. Population genomics of a forest fungus reveals high gene flow and climate adaptation signatures. Mol Ecol. 2022;31(7):1963–79. https://doi.org/10.1111/mec.16369.
11. Büntgen U, Kauserud H, Egli S. Linking climate variability to mushroom productivity and phenology. Front Ecol Environ. 2012;10(1):14–9. https://doi.org/10.1890/110064.
12. Boddy L, Büntgen U, Egli S, et al. Climate variation effects on fungal fruiting. Fungal Ecol. 2014;10:20–33. https://doi.org/10.1016/j.funeco.2013.10.006.
13. Koizumi T, Nara K. Population genetic consequences of habitat fragmentation in ectomycorrhizal fungi with different dispersal mechanisms: implications from ice-aged relict forests across the Japanese archipelago. BMC Ecol Evol. 2026;26(1). https://doi.org/10.1186/s12862-025-02475-8.
14. Nathan R, Muller-Landau HC. Spatial patterns of seed dispersal, their determinants and consequences for recruitment. Trends Ecol Evol. 2000;15(7):278–85. https://doi.org/10.1016/S0169-5347(00)01874-7.
15. Wright SJ, Trakhtenbrot A, Bohrer G, et al. Understanding strategies for seed dispersal by wind under contrasting atmospheric conditions. Proc Natl Acad Sci USA. 2008;105(49):19084–9. https://doi.org/10.1073/pnas.0802697105.
16. Zhang MZ, Xu JP, Callac P, et al. Insight into the evolutionary and domesticated history of the most widely cultivated mushroom Agaricus bisporus via mitogenome sequences of 361 global strains.

BMC Genomics. 2023;24(182). https://doi.org/10.1186/s12864-023-09257-w.

17. Bullock JM, Kenward RE, Hails R. Dispersal Ecology. Oxford: Oxford University Press; 2002.
18. Álvarez-Garrido L, Viñegla B, Hortal S, et al. Distributional shifts in ectomycorrizhal fungal communities lag behind climate-driven tree upward migration in a conifer forest-high elevation shrubland ecotone. Soil Biol Biochem. 2019;137:107545. https://doi.org/10.1016/j.soilbio.2019.107545.
19. Allbee SA, Rogers HS, Sullivan LL. The effects of dispersal, herbivory, and competition on plant community assembly. Ecology. 2022;104(1):e3859. https://doi.org/10.1002/ecy.3859.
20. Carteron A, Cantera I, Guerrieri A, et al. Dynamics and drivers of mycorrhizal fungi after glacier retreat. New Phytol. 2024;242:1739–52. https://doi.org/10.1111/nph.19682.
21. Hessenauer P, Feau N, Heinzelmann R, Hamelin RC. Genomic exploration of climate-driven evolution and evolutionary convergence in forest pathogens. Genome Biol Evol. 2025;17:evaf069. https://doi.org/10.1093/gbe/evaf069.
22. Wang XW, Varga T, Li QS, et al. Analyses of trait evolution and diversification reveal multiple adaptive periods in the fungal order Hymenochaetales. Mycosphere. 2025;16:517–35. https://doi.org/10.1101/2024.06.06.597693.
23. Zhu QL, Lin Y, Lyu XL, et al. Fungal strains with identical genomes were found at a distance of 2000 kilometers after 40 years. J Fungi. 2022;8(11):1212. https://doi.org/10.3390/jof8111212.
24. Capblancq T, Fitzpatrick MC, Bay RA, et al. Genomic prediction of (Mal)adaptation across current and future climatic landscapes. Annu Rev Ecol Evol Syst. 2020;51:245–69. https://doi.org/10.1146/annurev-ecolsys-020720-042553.
25. Filipe JC, Rymer PD, Byrne M, et al. Signatures of natural selection in a foundation tree along mediterranean climatic gradients. Mol Ecol. 2022;31:1735–52. https://doi.org/10.1111/mec.16351.
26. Suda RA, Kubota S, Kumar V, et al. Population genomics reveals demographic history and climate adaptation in Japanese *Arabidopsis halleri*. Plant Cell Physiol. 2025;66(4):529–41. https://doi.org/10.1093/pcp/pcae113.
27. Cao L, Yang D, Zhang Q, et al. Population genetic structure of *Hymenopellis radicata* germplasm resources based on genome re-sequencing. Front Microbiol. 2024;15:1287641. https://doi.org/10.3389/fmicb.2024.1287641.
28. Ling ZL, Chen GT, Zhang MZ, et al. Genomic signatures of evolution and domestication in the button mushroom *Agaricus bisporus*. Curr Biol. 2026;36(2):506–21. https://doi.org/10.1016/j.cub.2025.12.008.
29. Ye SY, Zhang YB, Wu F, Liu HX. Multi-locus phylogeny reveals two new species of *Exidia* (Auriculariales, Basidiomycota) from China. Mycological Progress. 2020;19:859–68. https://doi.org/10.1007/s11557-020-01601-8.
30. Tohtirjap A, Hou SX, Rivoire B, et al. Two new species of *Exidia* sensu lato (Auriculariales, Basidiomycota) based on morphology and DNA sequences. Front Microbiol. 2023;13:1080290. https://doi.org/10.3389/fmicb.2022.1080290.

31. Jiang YT, Wang L, Zhou CQ, et al. Molecular phylogeny and morphology reveal a new species of *Exidia* (Auriculariaceae, Auriculariales) from Yunnan Province, China. Phytotaxa. 2025;689(1):27–39. https://doi.org/10.11646/phytotaxa.689.1.3.
32. Li WY, Tohtirjap A, Wu F, Gao L. Biological characteristics and domestication of *Exidia yadongensis*. Mycosystema. 2025;44(8):250033. https://doi.org/10.13346/j.mycosystema.250033.
33. Liers C, Pecyna MJ, Kellner H, et al. Substrate oxidation by dye-decolorizing peroxidases (DyPs) from wood- and litter-degrading agaricomycetes compared to other fungal and plant heme-peroxidases. Appl Microbiol Biotechnol. 2013;97(13):5839–49. https://doi.org/10.1007/s00253-012-4521-2.
34. Sedova A, Rucká L, Bojarová P, et al. Application potential of cyanide hydratase from *Exidia glandulosa*: free cyanide removal from simulated industrial effluents. Catalysts. 2021;11(11):1410. https://doi.org/10.3390/catal11111410.
35. Martínková L, Kulik N, Rucká L, et al. Biotransformation of free cyanide to formic acid by a cyanide hydratase–formamidase cascade reaction. Process Biochem. 2024;142:62–7. https://doi.org/10.1016/j.procbio.2024.04.009.
36. Nagy LG, Riley R, Tritt A, et al. Comparative genomics of early-diverging mushroom-forming fungi provides insights into the origins of lignocellulose decay capabilities. Mol Biol Evol. 2016;33(4):959–70. https://doi.org/10.1093/molbev/msv337.
37. Fang M, Wang X, Chen Y, et al. Genome sequence analysis of *Auricularia heimuer* combined with genetic linkage map. J Fungi. 2020;6(1):37. https://doi.org/10.3390/jof6010037.
38. Dai YT, Li X, Song B, et al. Genomic analyses provide insights into the evolutionary history and genetic diversity of *Auricularia* species. Front Microbiol. 2019;10:2255. https://doi.org/10.3389/fmicb.2019.02255.
39. Ma XX, Lu LX, Yao FJ, et al. High-quality genome assembly and multi-omics analysis of pigment synthesis pathway in *Auricularia cornea*. Front Microbiol. 2023;14:1211795. https://doi.org/10.3389/fmicb.2023.1211795.
40. He MQ, Cao B, Liu F, et al. Phylogenomics, divergence times and notes of orders in Basidiomycota. Fungal Divers. 2024;126:127–406. https://doi.org/10.1007/s13225-024-00535-w.
41. Liu B, Tremellales, Dacrymycetales. Flora Fungorum Sinicorum 2. Beijing: Science; 1992. pp. 1–93.
42. Teng SC. Fungi of china. Ithaca: Mycotaxon Ltd.; 1996. pp. 1–586.
43. Mao XL. The macrofungi in China. Zhengzhou: Henan Science Technology; 2000. pp. 1–719.
44. Li Y, Li TH, Yang ZL, et al. Atlas of chinese macrofungal resources. Zhengzhou: Central China Farmer's Publishing House; 2015. pp. 1–1351.
45. Wu F, Zhou LW, Yang ZL, et al. Resource diversity of Chinese macrofungi: edible, medicinal and poisonous species. Fungal Divers. 2019;98(1):1–76. https://doi.org/10.1007/s13225-019-00432-7.
46. Cui YJ, Wu YD, Jiang YH, et al. Diversity of macrofungi in southeast Xizang 1. The wooddecay fungi. Mycology. 2025;16(2):635–69. https://doi.org/10.1080/21501203.2024.2379476.

47. Lu JR, Lei L, Yu FM, et al. Diversity of macrofungi in southeast Xizang, China 2. Mycology. 2026;17(1):2525864. https://doi.org/10.1080/21501203.2025.2525864.
48. Zhang ZX, Shang YX, Liu QY, et al. Deciphering the evolutionary and taxonomic complexity of Diaporthales (Sordariomycetes, Ascomycota) through integrated phylogenomic and divergence time estimation. Fungal Divers. 2025;132:1–125. https://doi.org/10.1007/s13225-025-00551-4.
49. Andrews S. FastQC: a quality control tool for high throughput sequence data. Cambridge: Babraham Bioinformatics, Babraham Institute; 2010.
50. Chen SF, Zhou YQ, Chen YR, Gu J. Fastp: an ultra-fast all-in-one FASTQ preprocessor. Bioinformatics. 2018;34(17):884–90. https://doi.org/10.1093/bioinformatics/bty560.
51. Marçais G, Kingsford C. A fast, lock-free approach for efficient parallel counting of occurrences of k-mers. Bioinformatics. 2011;27(6):764–70. https://doi.org/10.1093/bioinformatics/btr011.
52. Vurture GW, Sedlazeck FJ, Nattestad M, et al. Genomescope: fast reference-free genome profiling from short reads. Bioinformatics. 2017;33(18):2202–4. https://doi.org/10.1093/bioinformatics/btx153.
53. Koren S, Walenz BP, Berlin K, et al. Canu: scalable and accurate long-read assembly via adaptive k-mer weighting and repeat separation. Genome Res. 2017;27(5):722–36. https://doi.org/10.1101/gr.215087.116.
54. Ardui S, Ameur A, Vermeesch JR, Hestan MS. Single molecule real-time (SMRT) sequencing comes of age: applications and utilities for medical diagnostics. Nucleic Acids Res. 2018;46(5):2159–68. https://doi.org/10.1093/nar/gky066.
55. Li H. Minimap2: pairwise alignment for nucleotide sequences. Bioinformatics. 2018;34(18):3094–100. https://doi.org/10.1093/bioinfor matics/bty191.
56. Guan DF, McCarthy SA, Wood J, et al. Identifying and removing haplotypic duplication in primary genome assemblies. Bioinformatics. 2020;36(9):2896–8. https://doi.org/10.1093/bioinformatics/btaa025.
57. Chakraborty M, Baldwin-Brown JG, Long AD, Emerson JJ. Contiguous and accurate de novo assembly of metazoan genomes with modest long read coverage. Nucleic Acids Res. 2016;44(19):e147. https://doi.org/10.1093/nar/gkw654.
58. Liu SB, Zhao H, Wu F. High-quality genome assembly and annotation of *Porodaedalea mongolica* and *Porodaedalea schrenkiana* provide insights into potential industrial and medical application. G3-Genes Genomes Genetics. 2025; 15(11): jkaf195. https://doi.org/10.1093/g3journal/jkaf195
59. Hu J, Fan JF, Sun ZY, Liu SL. NextPolish: a fast and efficient genome polishing tool for long-read assembly. Bioinformatics. 2020;36(7):2253–5. https://doi.org/10.1093/bioinformatics/btz891.
60. Shen W, Le S, Li Y, Hu FQ. SeqKit: a cross-platform and ultrafast toolkit for FASTA/Q file manipulation. PLoS ONE. 2016;11:e0163962. https://doi.org/10.1371/journal.pone.0163962.
61. Gurevich A, Saveliev V, Vyahhi N, Tesler G. QUAST: quality assessment tool for genome assemblies. Bioinformatics. 2013;29(8):1072–5. https://doi.org/10.1093/bioinformatics/btt086.

62. Simão FA, Waterhouse RM, Ioannidis P, et al. BUSCO: assessing genome assembly and annotation completeness with single-copy orthologs. Bioinformatics. 2015;31(19):3210–2. https://doi.org/10.1093/bioinformatics/btv351.
63. Tarailo-Graovac M, Chen N. Using RepeatMasker to identify repetitive elements in genomic sequences. Curr Protocols Bioinf. 2009;25(4). https://doi.org/10.1002/0471250953.bi0410s25. .10.1–4.10.14.
64. Xu Z, Wang H. LTR_FINDER: an efficient tool for the prediction of full-length LTR retrotransposons. Nucleic Acids Res. 2007;35(2):265–8. https://doi.org/10.1093/nar/gkm286.
65. Ou S, Jiang N. LTR_retriever: a highly accurate and sensitive program for identification of long terminal repeat retrotransposons. Plant Physiol. 2018;176(2):1410–22. https://doi.org/10.1104/pp.17.01310.
66. Flynn JM, Hubley R, Goubert C, et al. RepeatModeler2 for automated genomic discovery of transposable element families. Proc Natl Acad Sci USA. 2020;117(17):9451–7. https://doi.org/10.1073/pnas.1921046117.
67. Benson G. Tandem repeats finder: a program to analyze DNA sequences. Nucleic Acids Res. 1999;27(2):573–80. https://doi.org/10.1093/nar/27.2.573.
68. Nawrocki EP, Eddy SR. Infernal 1.1: 100-fold faster RNA homology searches. Bioinformatics. 2013;29(22):2933–5. https://doi.org/10.1093/bioinformatics/btt509.
69. Lagesen K, Hallin P, Rødland EA, et al. RNAmmer: consistent and rapid annotation of ribosomal RNA genes. Nucleic Acids Res. 2007;35(9):3100–8. https://doi.org/10.1093/nar/gkm160.
70. Chan PP, Lin BY, Mak AJ, Lowe TM. tRNAscan-SE 2.0: improved detection and functional classification of transfer RNA genes. Nucleic Acids Res. 2021;49(16):9077–96. https://doi.org/10.1093/nar/gkab688.
71. Quinlan AR. BEDTools: the Swiss-army tool for genome feature analysis. Current Protocols Bioinformatics. 2014; 47: 11.12.1–11.12.34. https://doi.org/10.1002/0471250953.bi1112s47
72. Stanke M, Diekhans M, Baertsch R, Haussler D. Using native and syntenically mapped cDNA alignments to improve de novo gene finding. Bioinformatics. 2008;24(5):637–44. https://doi.org/10.1093/bioinformatics/btn013.
73. Keilwagen J, Wenk M, Erickson JL, et al. Using intron position conservation for homology-based gene prediction. Nucleic Acids Res. 2016;44(9):e89. https://doi.org/10.1093/nar/gkw092.
74. Haas BJ, Salzberg SL, Zhu W, et al. Automated eukaryotic gene structure annotation using EVidenceModeler and the program to assemble spliced alignments. Genome Biol. 2008;9:R7. https://doi.org/10.1186/gb-2008-9-1-r7.
75. Li H, Durbin R. Fast and accurate short read alignment with Burrows-Wheeler transform. Bioinformatics. 2009;25(14):1754–60. https://doi.org/10.1093/bioinformatics/btp324.
76. Li H, Handsaker B, Wysoker A, et al. The sequence alignment/map format and SAMtools. Bioinformatics. 2009;25(16):2078–9. https://doi.org/10.1093/bioinformatics/btp352.

77. Okonechnikov K, Conesa A, García-Alcalde F. Bioinformatics. 2016;32(2):292–4. https://doi.org/10.1093/bioinformatics/btv566. Qualimap2: advanced multi-sample quality control for high-throughput sequencing data.
78. McKenna A, Hanna M, Banks E, et al. The genome analysis toolkit: a MapReduce framework for analyzing next-generation DNA sequencing data. Genome Res. 2010;20(9):1297–303. https://doi.org/10.1101/gr.107524.110.
79. Danecek P, Auton A, Abecasis G, et al. The variant call format and VCFtools. Bioinformatics. 2011;27(15):2156–8. https://doi.org/10.1093/bioinformatics/btr330.
80. Wang K, Li MY, Hakonarson H. ANNOVAR: functional annotation of genetic variants from high-throughput sequencing data. Nucleic Acids Res. 2010;38(16):e164. https://doi.org/10.1093/nar/gkq603.
81. Bradbury PJ, Zhang Z, Kroon DE, et al. TASSEL: Software for association mapping of complex traits in diverse samples. Bioinformatics. 2007;23(19):2633–5. https://doi.org/10.1093/bioinformatics/btm308.
82. Kozlov AM, Darriba D, Flouri T, et al. RAxML-NG: a fast, scalable and user-friendly tool for maximum likelihood phylogenetic inference. Bioinformatics. 2019;35(21):4453–5. https://doi.org/10.1093/bioinformatics/btz305.
83. Floudas D, Binder M, Riley R. The Paleozoic origin of enzymatic lignin decomposition reconstructed from 31 fungal genomes. Science. 2012;336(6089):1715–9. https://doi.org/10.1126/science.1221748.
84. Purcell S, Neale B, Todd-Brown K, et al. PLINK: a tool set for whole-genome association and population-based linkage analyses. Am J Hum Genet. 2007;81(3):559–75. https://doi.org/10.1086/519795.
85. Alexander DH, Novembre J, Lange K. Fast model-based estimation of ancestry in unrelated individuals. Genome Res. 2009;19(9):1655–64. https://doi.org/10.1101/gr.094052.109.
86. Zhang C, Dong SS, Xu JY, et al. PopLDdecay: a fast and effective tool for linkage disequilibrium decay analysis based on variant call format files. Bioinformatics. 2019;35(10):1786–8. https://doi.org/10.1093/bioinformatics/bty875.
87. Pickrell JK, Pritchard JK. Inference of population splits and mixtures from genome-wide allele frequency data. PLoS Genet. 2012;8(11):e1002967. https://doi.org/10.1038/npre.2012.6956.1.
88. Li MZ, Tian SL, Jin L, et al. Genomic analyses identify distinct patterns of selection in domesticated pigs and Tibetan wild boars. Nat Genet. 2013;45:1431–8. https://doi.org/10.1038/ng.2811.
89. Korneliussen TS, Moltke I, Albrechtsen A, Nielsen R. Calculation of Tajima's D and other neutrality test statistics from low depth next-generation sequencing data. BMC Bioinformatics. 2013;14:289. https://doi.org/10.1186/1471-2105-14-289.
90. Zhou Y, Zhao XB, Li YW, et al. Triticum population sequencing provides insights into wheat adaptation. Nat Genet. 2020;52:1412–22. https://doi.org/10.1038/s41588-020-00722-w.

91. Danecek P, Bonfield JK, Liddle J, et al. Twelve years of SAMtools and BCFtools. Gigascience. 2021;10(2):giab008. https://doi.org/10.1093/gigascience/giab008.
92. Huerta-Cepas J, Szklarczyk D, Heller D, et al. eggNOG 5.0: a hierarchical, functionally and phylogenetically annotated orthology resource based on 5090 organisms and 2502 viruses. Nucleic Acids Res. 2019;47(D1):D309–14. https://doi.org/10.1093/nar/gky1085.
93. Bao DP. Research progress and insights of the biological properties of edible basidiomycete dikaryon. Mycosystema. 2024;43:14–29. https://doi.org/10.13346/j.mycosystema.230319.
94. Bao DP, Xu JP, Pan YJ, Tan Q. Dynamic relationships between dikaryon and monokaryon in heterothallic edible fungi. Acta Edulis Fungi. 2024; 31: 1–11. https://doi.org/10.16488/j.cnki.1005-9873. 2024.04.001.
95. Nieuwenhuis BPS, Aanen DK. Sexual selection in fungi. J Evol Biol. 2012;25(12):2397–411. https://doi.org/10.1111/jeb.12017.
96. Ma JX, Wang H, Jin C, et al. Whole genome sequencing and annotation of *Daedaleopsis sinensis*, a wood-decaying fungus significantly degrading lignocellulose. Front Bioeng Biotechnol. 2024;11:1325088. https://doi.org/10.3389/fbioe.2023.1325088.
97. Samarasinghe H, You M, Jenkinson TS, et al. Hybridization facilitates daptive evolution in two major fungal pathogens. Genes. 2020;11:101. https://doi.org/10.3390/genes11010101.
98. Li Z, Zhu Z, Qian K, et al. Intraspecific diploidization of a halophyte root fungus drives heterosis. Nat Commun. 2024;15:5872. https://doi.org/10.1038/s41467-024-49468-7.
99. Mixão V, Saus E, Hagen F, et al. A yeast love triangle: multiple hybridizations shape genome evolution in the *Pichia cactophila* species complex. Mycosphere. 2024;15(1):1083–109. https://doi.org/10.5943/mycosphere/15/1/9.
100. Cho Y, Seo CW, Jung PE, Lim YW. Global phylogeographical distribution of *Gloeoporus dichrous*. PLoS ONE. 2023;18(7):e0288498. https://doi.org/10.1371/journal.pone.0288498.
101. Li H, Xu J, Wang S, et al. Genetic differentiation and widespread mitochondrial heteroplasmy among geographic populations of the gourmet mushroom *Thelephora ganbajun* from Yunnan, China. Genes. 2022;13(5):854. https://doi.org/10.3390/genes13050854.
102. Hua R, Chen Z, Fu W. An overview of wild edible fungi resource conservation and its utilization in Yunnan. J Agricultural Sci. 2017;9:158–69. https://doi.org/10.5539/jas.v9n5p158.
103. Fu ZQ, Liu G, Wang LX. Assessment of potential human health risk of trace element in wild edible mushroom species collected from Yunnan Province, China. Environ Sci Pollut Res. 2020;27:29218–27. https://doi.org/10.1007/s11356-020-09242-w.
104. Punttila P, Ihalainen A. METSOn jäljillä - Etelä-Suomen metsien monimuotoisuusohjelman tutkimusraportti. Ministry of Agriculture, Ministry of the Environment. Helsinki: Finnish Forest Research Institute and Finnish Environment Institute; 2006.
105. Hao T, Guillera-Arroita G, May TW, et al. Using species distribution models for fungi. Fungal Biology Reviews. 2020;34(2):74–88. https://doi.org/10.1016/j.fbr.2020.01.002.

106. Chen JH, Shen S, Zhou LW. Modeling current geographic distribution and future range shifts of *Sanghuangporus* under multiple climate change scenarios in China. Front Microbiol. 2022;13:1064451. https://doi.org/10.3389/fmicb.2022.1064451.

107. Kaldis P, Life Sciences CMLS. 1999; 55: 284–96. https://doi.org/10.1007/s000180050290

108. Hofmann C, Shepelev M, Chernoff J. The genetics of PAK. J Cell Sci. 2004;117:4343–54. https://doi.org/10.1242/jcs.01392.

109. Park G, Servin JA, Turner GE, et al. Global analysis of serine–threonine protein kinase genes in *Neurospora crassa*. Eukaryot Cell. 2011;10:1553–64. https://doi.org/10.1128/ec.05140-11.

110. Zhao ZS, Manser E. PAK family kinases: physiological roles and regulation. Cell Logist. 2012;2:59–68. https://doi.org/10.4161/cl.21912.

111. Cotteret S, Chernoff J. The evolutionary history of effectors downstream of Cdc42 and Rac. Genome Biol. 2002;3(2):REVIEWS0002. https://doi.org/10.1186/gb-2002-3-2-reviews0002.

112. Scheffer J, Chen C, Heidrich P, et al. A CDC42 homologue in *Claviceps purpurea* is involved in vegetative differentiation and is essential for pathogenicity. Eukaryot Cell. 2005;4(7):1228–38. https://doi.org/10.1128/EC.4.7.1228-1238.2005.

113. Li H, Barker BM, Grahl N, et al. The small GTPase RacA mediates intracellular reactive oxygen species production, polarized growth, and virulence in the human fungal pathogen *Aspergillus fumigatus*. Eukaryot Cell. 2011;10(2):174–86. https://doi.org/10.1128/EC.00288-10.

114. Zhang X, Wang Z, Jiang C, Xu JR. Regulation of biotic interactions and responses to abiotic stresses by MAP kinase pathways in plant pathogenic fungi. Stress Biology. 2021;1(1):5. https://doi.org/10.1007/s44154-021-00004-3.

115. Busto JV, Wedlich-Söldner R. Integration through separation – the role of lateral membrane segregation in nutrient uptake. Front Cell Dev Biology. 2019;7:97. https://doi.org/10.3389/fcell.2019.00097.

116. Barata-Antunes C, Alves R, Talaia G, et al. Endocytosis of nutrient transporters in fungi: The ART of connecting signaling and trafficking. Comput Struct Biotechnol J. 2021;19:1713–37. https://doi.org/10.1016/j.csbj.2021.03.013.

117. Saraste M. Oxidative phosphorylation at the fin de siècle. Science. 1999;283:1488–93. https://doi.org/10.1126/science.283.5407.1488.

118. Stenger M, Le DT, Klecker T, Westermann B. Systematic analysis of nuclear gene function in respiratory growth and expression of the mitochondrial genome in *S. cerevisiae*. Microbial Cell. 2020; 7(9): 234–249. https://doi.org/10.15698/mic2020.09.729

119. Bleier L, Wittig I, Heide H, et al. Generator-specific targets of mitochondrial reactive oxygen species. Free Radic Biol Med. 2015;78:1–10. https://doi.org/10.1016/j.freeradbiomed.2014.10.511.

120. Schikora-Tamarit MÀ, Marcet-Houben M, Nosek J, Gabaldón T. Shared evolutionary footprints suggest mitochondrial oxidative damage underlies multiple complex I losses in fungi. Open Biology. 2021;11(4):200362. https://doi.org/10.1098/rsob.200362.

121. Singh S, Singh R. High-altitude clear-sky direct solar ultraviolet irradiance at Leh and Hanle in the western Himalayas: Observations and model calculations. J Geophys Research-Atmospheres. 2004;109:D19201. https://doi.org/10.1029/2004JD004854.
122. Stres B, Sul WJ, Murovec B, Tiedje JM. Recently deglaciated high-altitude soils of the Himalaya: diverse environments, heterogenous bacterial communities and long-range dust inputs from the upper troposphere. PLoS ONE. 2014;9(1):101371. https://doi.org/10.1371/journal.pone.0076440.
123. Wang YL, Li L, Paudel BR, Zhao JL. Genomic insights into high-altitude adaptation: a comparative analysis of *Roscoea alpina* and *R. purpurea* in the himalayas. Int J Mol Sci. 2024;25(4):2265. https://doi.org/10.3390/ijms25042265.
124. Garcia D, Shaw RJ. AMPK: mechanisms of cellular energy sensing and restoration of metabolic balance. Mol Cell. 2017;66(6):789–800. https://doi.org/10.1016/j.molcel.2017.05.032.
125. Li YJ, Yan PF, Lu XJ, et al. Involvement of PaSNF1 in fungal development, sterigmatocystin biosynthesis, and lignocellulosic degradation in the filamentous fungus *Podospora anserina*. Front Microbiol. 2020;11:1038. https://doi.org/10.3389/fmicb.2020.01038.
126. Heinz D, Krotova E, Hamann A, Osiewacz HD. Simultaneous ablation of the catalytic AMPK α-Subunit SNF1 and mitochondrial matrix protease CLPP results in pronounced lifespan extension. Front Cell Dev Biology. 2021;9:616520. https://doi.org/10.3389/fcell.2021.616520.
127. Longo VD, Fabrizio P, Visions. & Reflections¶Regulation of longevity and stress resistance: a molecular strategy conserved from yeast to humans? Cellular and Molecular Life Sciences. 2002; 59(6): 903–8. https://doi.org/10.1007/s00018-002-8477-8
128. Malik AA, Martiny JBH, Brodie EL, et al. Defining trait-based microbial strategies with consequences for soil carbon cycling under climate change. Int Soc Microb Ecol J. 2020;14:1–9. https://doi.org/10.1038/s41396-019-0510-0.
129. Zhou J, Wang J, Yu JQ, Chen ZX. Role and regulation of autophagy in heat stress responses of tomato plants. Front Plant Sci. 2014;5:174. https://doi.org/10.3389/fpls.2014.00174.
130. Teoh TC, Rizman-Idid M, Wong HJ, et al. Transcriptomic evidence of base and nucleotide excision repair mechanisms in response to UV-B radiation in an arctic fungus *Pseudogymnoascus australis* Strain HNDR4. Chiang Mai J Sci. 2024;51(2):e2024029. https://doi.org/10.12982/CMJS.2024.029.
131. Staszczak M. The role of the ubiquitin-proteasome system in the response of the ligninolytic fungus Trametes versicolor to nitrogen deprivation. Fungal Genet Biol. 2008;45(3):328–37. https://doi.org/10.1016/j.fgb.2007.10.017.

Figures

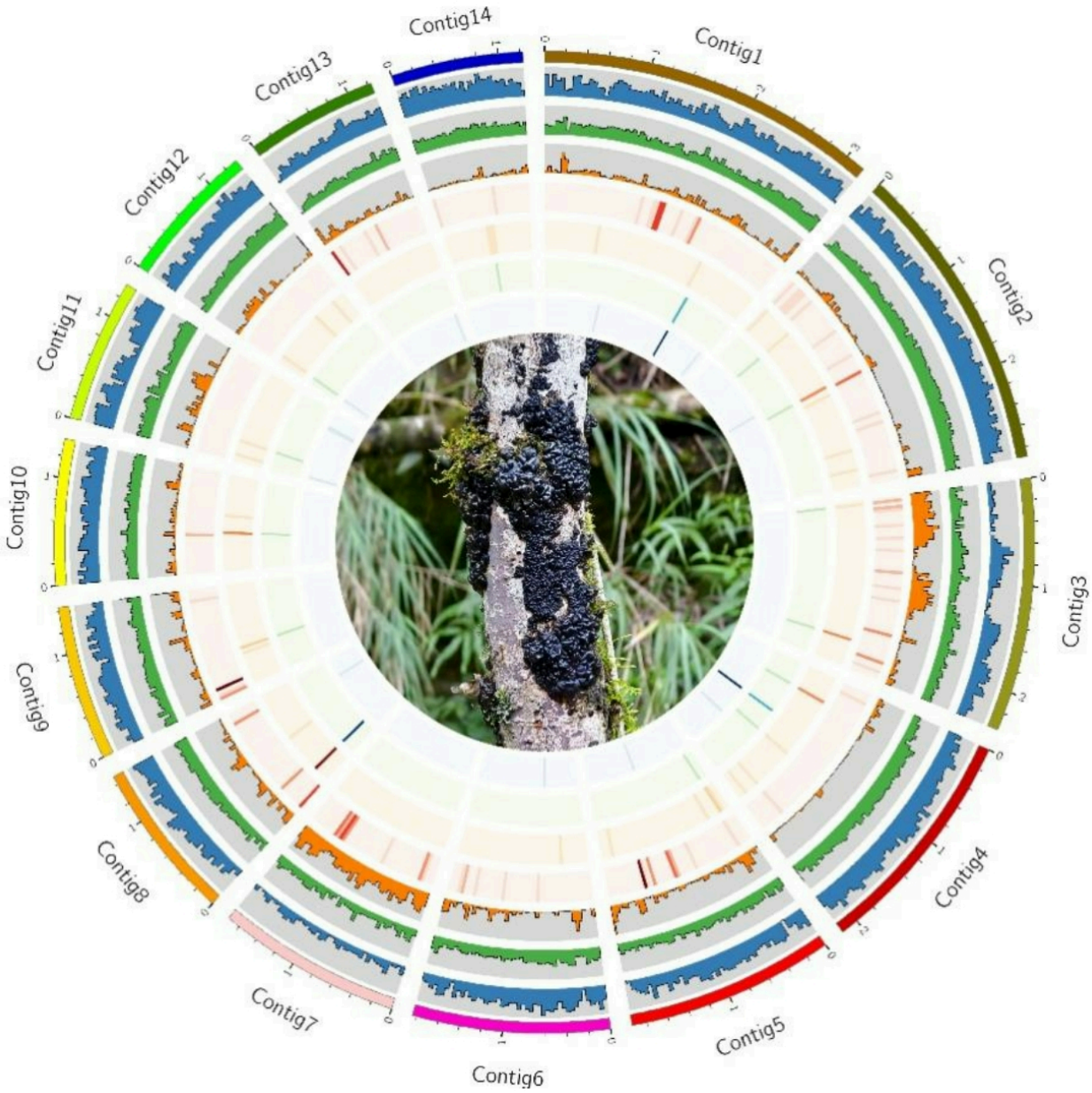


Figure 1

Genome assembly characteristics of *Exidia glandulosa* with a window size of 50 kb. From outside to inside: (1) contigs (length > 1.5 Mb); (2) protein-coding genes density; (3) GC content; (4) average distribution density of transposable elements; (5) gene density of four categories (tandem repeats, rRNA, snRNA, and tRNA), each represented by one of the four inner circles.



Figure 2

Basidiomata morphology of *Exidia glandulosa* under different climatic conditions in China. (**A–E**) temperate climate; (**F-J**) subtropical climate; (**K-P**) plateau climate.

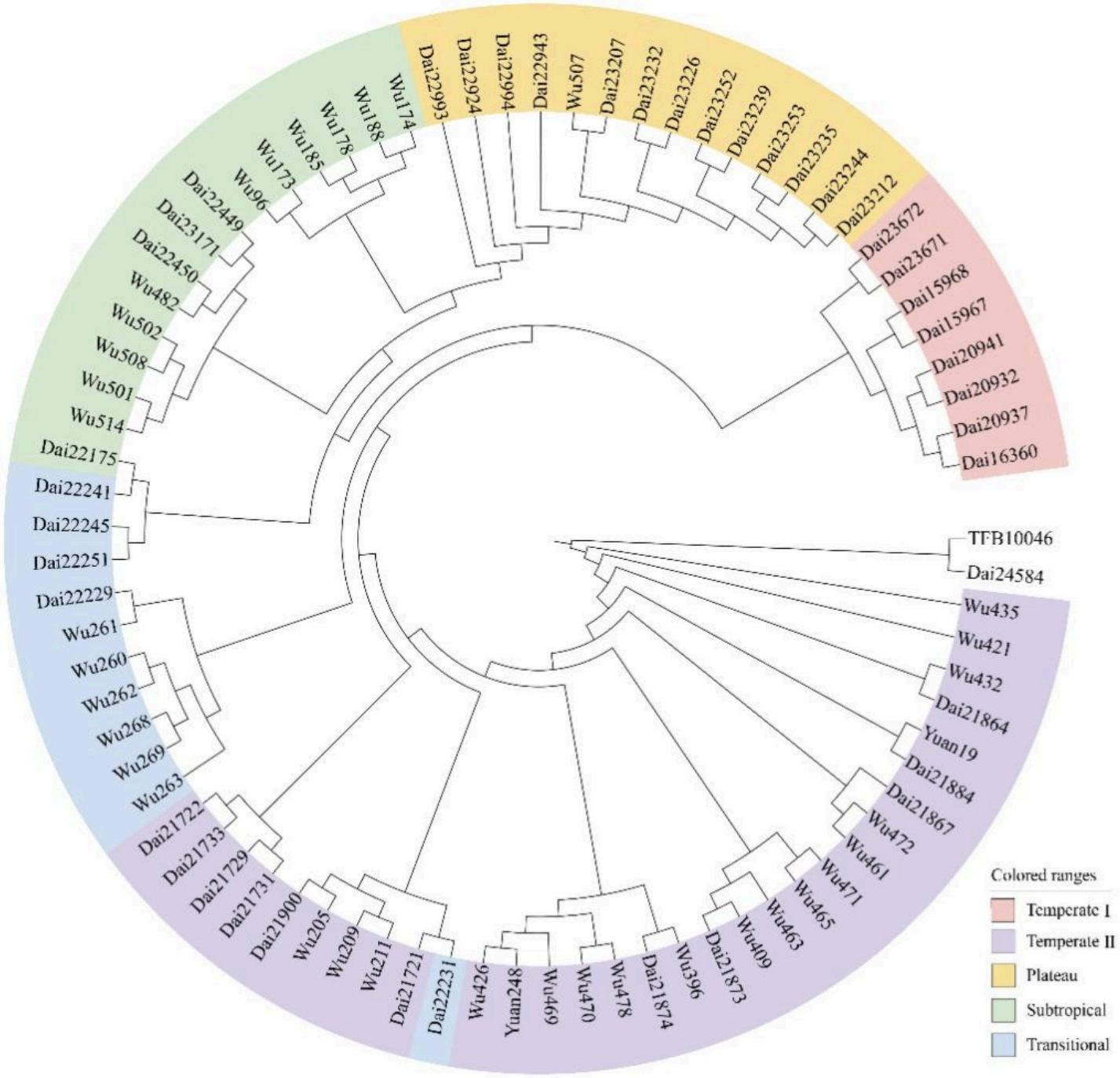


Figure 3

Phylogenetic analysis based on SNPs, with different color labels representing the population groups assignments of the samples.

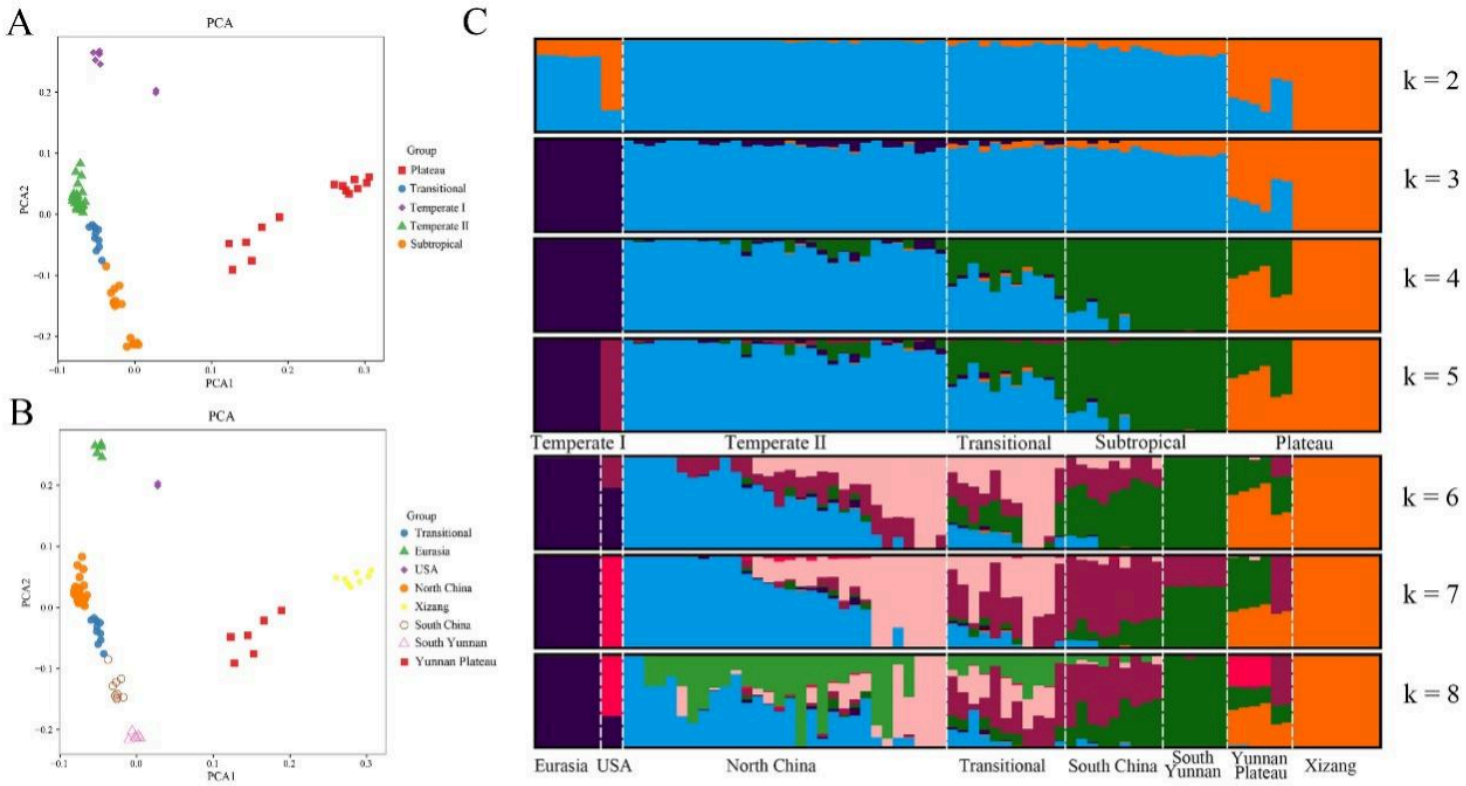


Figure 4

Principal component analysis: (**A**) marked by climate; (**B**) marked by region. (**C**) Population structure analysis (K = 2–8).

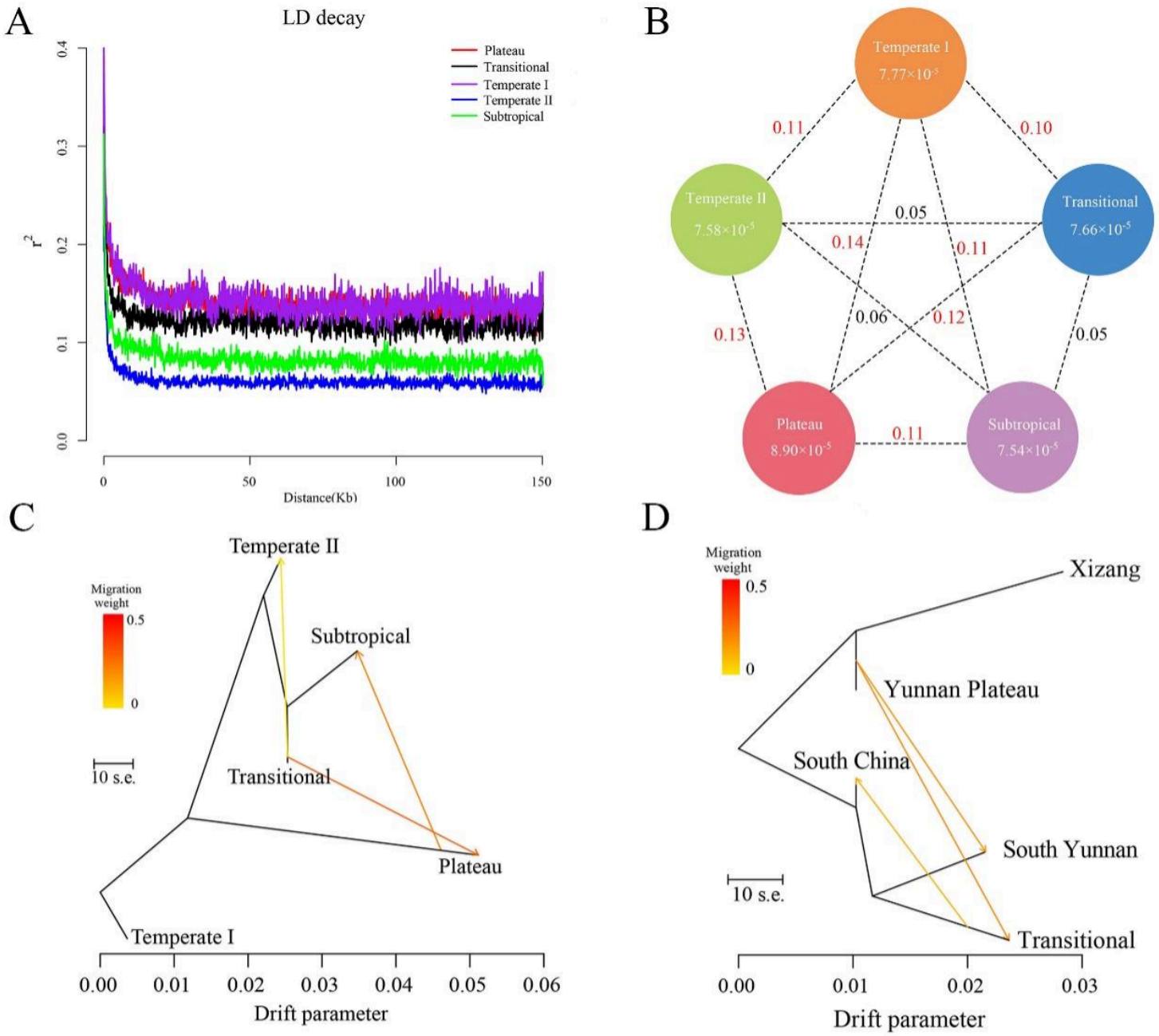


Figure 5

(**A**) Linkage disequilibrium analysis. (**B**) Pi of each population and Fst between populations. (**C**) Gene flow among five populations. (**D**) Gene flow among five subpopulations.

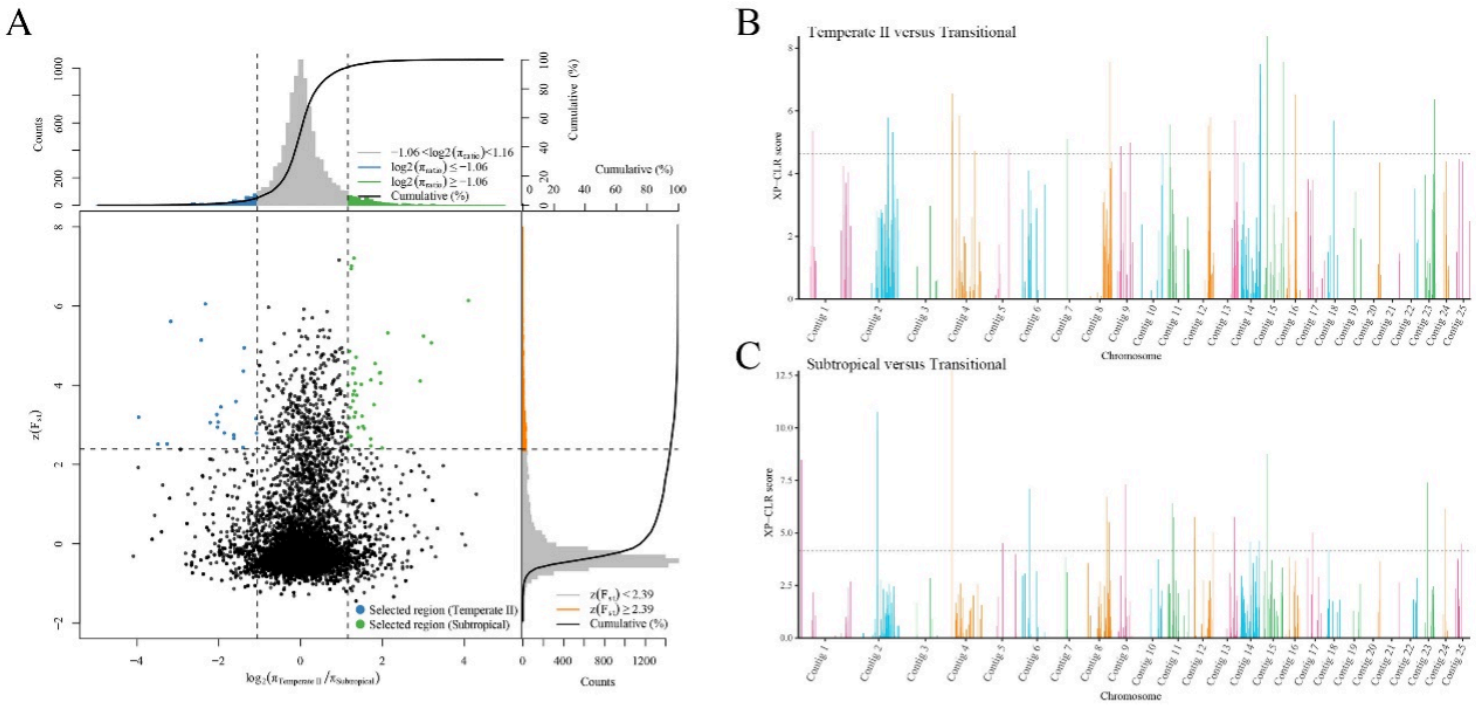


Figure 6

(**A**) Selected regions identified by joint Fst and Pi screening. Blue dots: Temperate II population. Green dots: Subtropical population. Manhattan plots of XP-CLR scores: (**B**) Temperate II population vs. Transitional population; (**C**) Subtropical population vs. Transitional population. Dashed line, top 1% threshold.

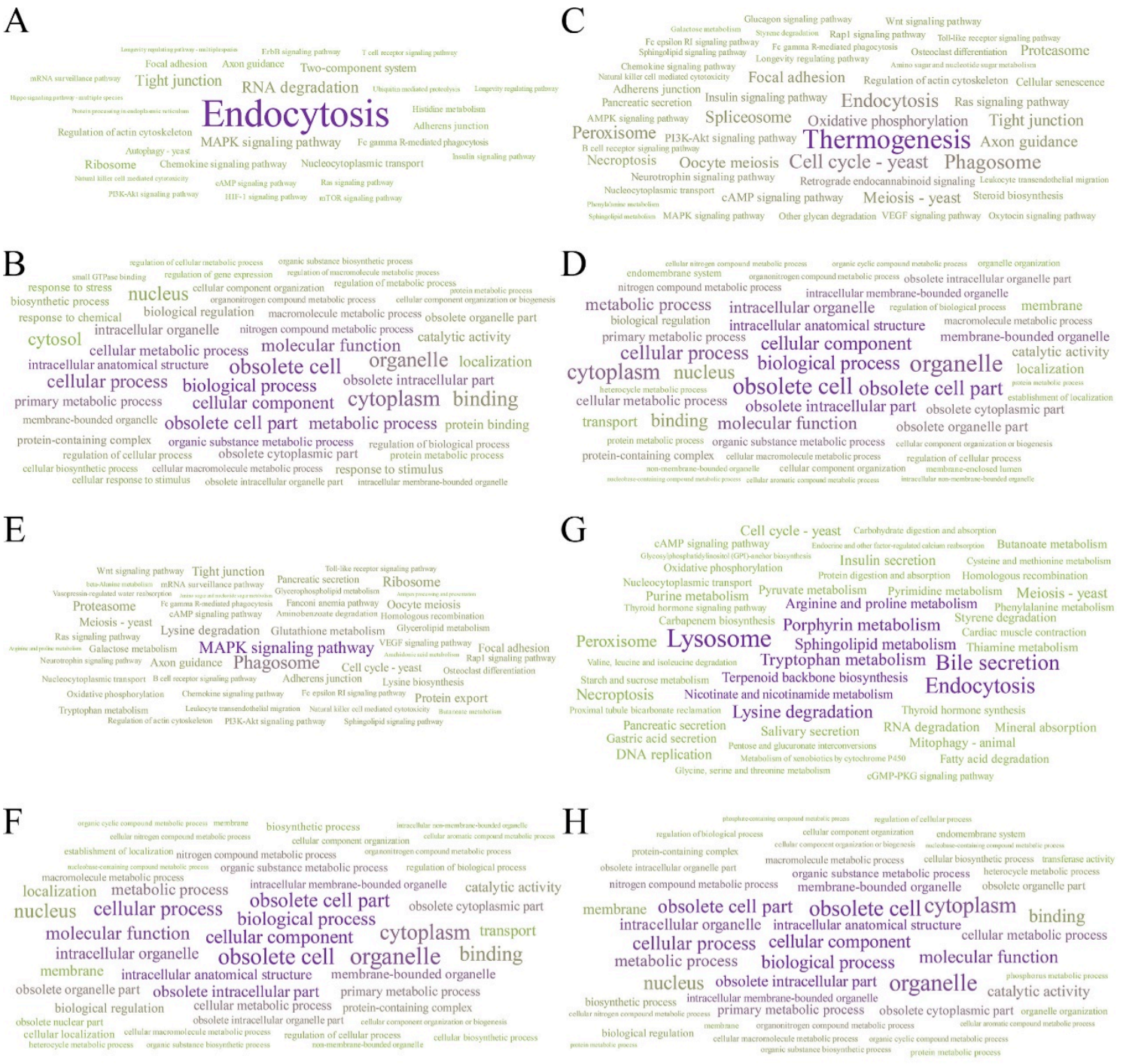


Figure 7

(**A–D**) Annotation of genes extracted by joint Fst and Pi selection. (**E–H)**Annotation of genes extracted by XP-CLR selection. KEGG annotations: Temperate II (**A** and **E**) and Subtropical (**C** and **G**) populations; GO annotations: Temperate II (**B** and **F**) and Subtropical (**D**and **H**) populations.

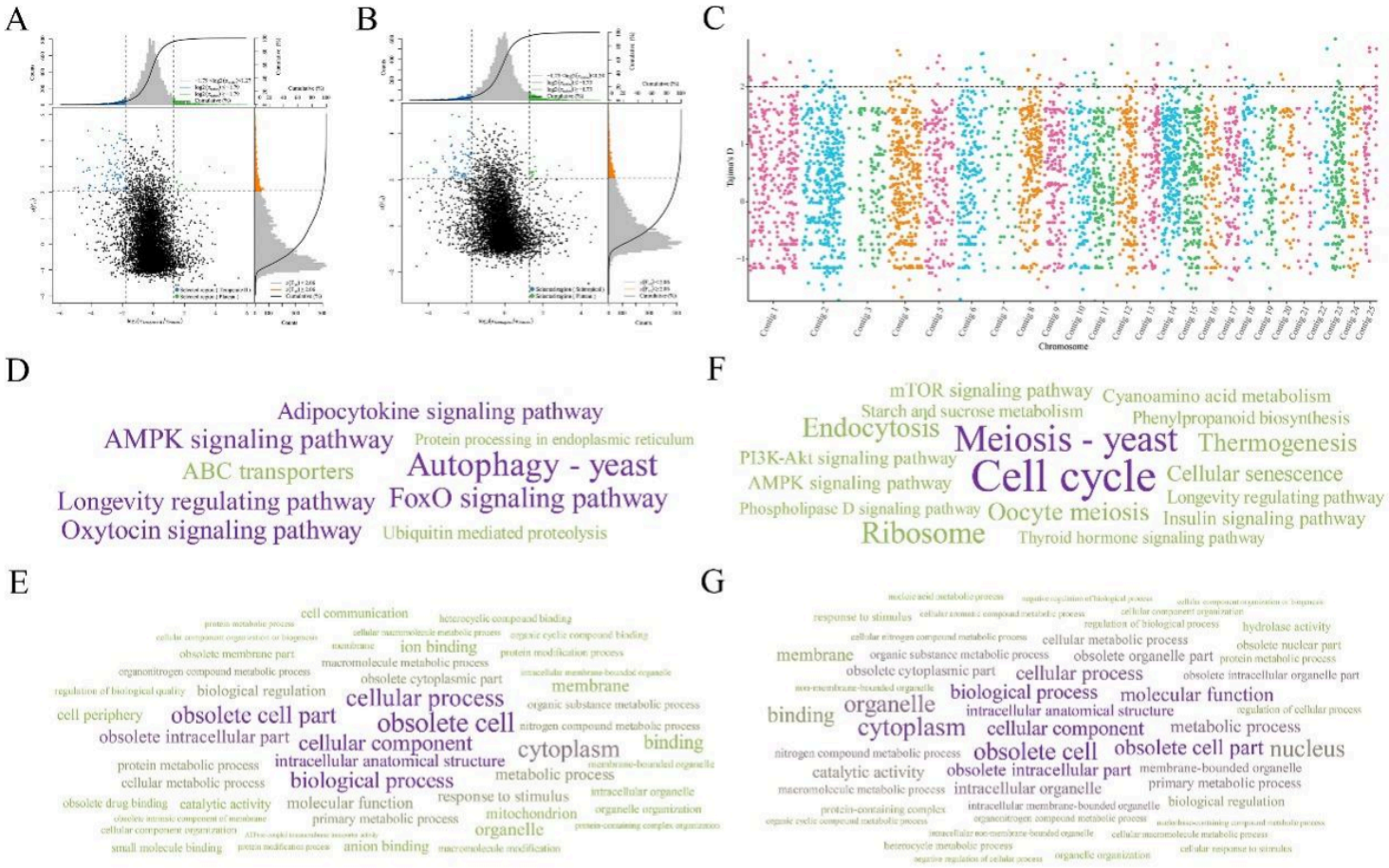


Figure 8

Selected regions identified by joint Fst and Pi screening. The overlapping regions between the two comparisons were taken as the final selected regions of the Plateau population. (**A**) Blue dots: Temperate II population. Green dots: Plateau population. (**B**) Blue dots: Subtropical population. Green dots: Plateau population. (**C**) Manhattan plot of Tajima's D for the Plateau population. Dashed line, threshold of Tajima's D > 2 for selected regions. KEGG (**D**) and GO (**E**) annotation of genes extracted by joint Fst and Pi selection. KEGG (**F**) and GO (**G**) annotation of genes extracted by Tajima's D selection.

Supplementary Files

This is a list of supplementary files associated with this preprint. Click to download.

- Supplementarymaterial1.xls
- Supplementarymaterial2.doc